Thermodynamics of $L1_0$ ordering in FePt nanoparticles studied by Monte Carlo simulations based on an analytic bond-order potential

Michael Müller,* Paul Erhart, and Karsten Albe
Institut für Materialwissenschaft, Technische Universität Darmstadt, D-64287 Darmstadt, Germany
(Received 26 January 2007; revised manuscript received 4 April 2007; published 15 October 2007)

The size dependence of the order-disorder transition in FePt nanoparticles with an $L1_0$ structure is investigated by means of Monte Carlo simulations based on an analytic bond-order potential for FePt. A cross parametrization for the Fe-Pt interaction is proposed, which complements existing potentials for the constituents Fe and Pt. This FePt potential properly describes structural properties of ordered and disordered phases, surface energies, and the $L1_0$ to $A1$ transition temperature in bulk FePt. The potential is applied for examining the ordering behavior in small particles. The observed lowering of the order-disorder transition temperature with decreasing particle size confirms previous lattice-based Monte Carlo simulations [M. Müller and K. Albe, Phys. Rev. B **72**, 094203 (2005)]. Although a distinctly higher amount of surface induced disorder is found in comparison to previous studies based on lattice-type Hamiltonians, the presence of lattice strain caused by the tetragonal distortion of the $L1_0$ structure does not have a significant influence on the depression of the ordering temperature with decreasing particle size.

DOI: 10.1103/PhysRevB.76.155412 PACS number(s): 61.46.Df, 34.20.Cf, 61.82.Bg, 64.60.Cn

I. INTRODUCTION

In the attempt to increase the areal density of magnetic data storage media, research interest has been directed toward the FePt alloy in the chemically ordered, face centered tetragonal $L1_0$ structure. Due to its high magnetocrystalline anisotropy, it offers the prospect of reducing the dimension of the magnetic units (grains, particles) to a few nanometers, while maintaining thermal stability of the magnetization direction.[1] Possible applications for FePt media comprise thin films for perpendicular recording,[2,3] as well as arrays of monodisperse nanoparticles,[4,5] the latter providing the potential for highest recording densities.

For the preparation of FePt nanoparticles, different synthesis routes are discussed in literature, including a chemical synthesis from the solution phase,[4,5] the preparation by evaporation or sputtering techniques,[6,7] and gas-phase preparation.[8] For producing highly ordered, monodispersed FePt particles, however, a number of challenges still have to be overcome. In the case of the solution phase synthesis route, for example, chemical ordering is typically not observed in the as-prepared particles, and a postannealing process at temperatures around 800 K is required for a transformation into the $L1_0$ structure.[9] Annealing processes lead to an increased internal order, but are usually accompanied by particle coalescence and sintering.[8,9] In contrast, isolated particles have been observed to remain in the disordered state even after heat treatment.[7,10,11]

The particle preparation from the gas phase opens an alternative synthesis route with a thermal annealing step of the particles prior to deposition.[8] The formation of the $L1_0$ order, however, has only been achieved for processing conditions with high pressures of the background gas, where coalescence occurs.[8] For lower gas pressures, multiply twinned icosahedral particles are typically formed, in which chemical ordering could not be established.

The absence of the $L1_0$ order in thermally annealed particles is not consistent with the FePt bulk phase diagram, where the disordered face centered cubic (fcc) $A1$ phase is thermodynamically stable only at temperatures above 1573 K.[12] Another intriguing finding in this context is that gas-phase prepared particles irradiated by ion beams also remain disordered, although the irradiation provides sufficient energy for transforming the particles from a multiply twinned into a single crystalline structure.[13] To date, it is not clear whether the experimental difficulties in producing chemically ordered FePt nanoparticles exist because the thermodynamic ordering temperature is reduced in small particles or whether a kinetic barrier impedes the $A1$ to $L1_0$ transformation.

Theoretically, the size dependence of the order-disorder transition temperature T_c has been investigated by various lattice-based Monte Carlo (MC) simulations.[14–17] All studies come univocally to the conclusion that T_c is lowered with decreasing particle size, but is still above the typical postannealing temperatures of about 800 K.[16] Lattice-based Hamiltonians, however, do not account for surface relaxation and internal strain, which can have a major influence on the ordering transition temperature.[3] Apart from ordering phenomena, the structural stability of multiply twinned FePt particles[8,18,19] is another issue which cannot be addressed by a lattice-based model. Thus, it is desirable to apply a continuous interatomic potential for the FePt system, which allows us to account for strain effects in atomistic simulations and can be used for validating the previously reported results based on lattice Hamiltonians.

In this work, we describe the development of such an interatomic potential for Fe-Pt. We apply the angular dependent analytic bond-order potential (ABOP) formalism, which has been successfully employed for modeling transition metals with a variety of crystal structures. Potentials exist for fcc platinum,[20,21] body centered cubic (bcc) iron,[22] and tungsten,[23] as well as hexagonal close packed zinc.[24] Important features of the potentials for pure iron and platinum are, for example, the bcc to fcc phase transition in Fe (Ref. 22) and the high stacking-fault/twin-boundary energy as well as the low elastic anisotropy ratio in Pt.[21] The parametrization of the Fe-Pt cross potential can therefore be built upon a

solid description of the boundary phases. As an application, the problem of the size dependence of the thermodynamic ordering temperature in small FePt particles is revisited by off-lattice MC simulations based on this newly developed bond-order potential for Fe-Pt.

The paper is organized as follows. In the first part, a short outline of the functional form of the bond-order formalism is given, and the fitting procedure of the Fe-Pt cross potential is described. Subsequently, the properties of the Fe-Pt parametrization are summarized and compared to a recent FePt potential based on the modified embedded atom method.[25] In the second part, the ABOP is applied in analyzing the ordering behavior of FePt nanoparticles. The results are discussed in comparison with our previous study based on a lattice Ising-type Hamiltonian.[16]

II. BOND-ORDER FORMALISM

The functional form of the analytic bond-order potential is summarized by the following equations. The physical background is described in Refs. 20 and 26–29.

The potential energy is written as a sum over individual bond energies

$$E = \sum_{i<j} f_{ij}^{c}(r_{ij}) \left[V_{ij}^{R}(r_{ij}) - \frac{b_{ij} + b_{ji}}{2} V_{ij}^{A}(r_{ij}) \right]. \tag{1}$$

The pairlike repulsive and attractive terms are taken as Morselike pair potentials

$$V^{R}(r) = \frac{D_0}{S-1} \exp[-\beta\sqrt{2S}(r - r_0)],$$

$$V^{A}(r) = \frac{SD_0}{S-1} \exp[-\beta\sqrt{2/S}(r - r_0)]. \tag{2}$$

Here, S is an adjustable parameter, while D_0 denotes the dimer bond energy and r_0 the dimer bond length. The parameter β can be determined from the ground-state oscillation frequency of the dimer. The interaction range is determined by the cutoff function

$$f^{c}(r) = \begin{cases} 1, & r \leqslant R - D \\ \frac{1}{2} - \frac{1}{2} \sin\left[\frac{\pi}{2}(r - R)/D \right], & |R - r| \leqslant D \\ 0, & r \geqslant R + D, \end{cases} \tag{3}$$

where R and D are adjustable parameters. Three-body contributions and angularity enter the energy function via the bond-order parameter b_{ij}

$$b_{ij} = (1 + \chi_{ij})^{-1/2}, \tag{4}$$

$$\chi_{ij} = \sum_{k \neq i,j} f_{ik}^{c}(r_{ik}) g_{ik}(\theta_{ijk}) \exp[2\mu_{ik}(r_{ij} - r_{ik})]. \tag{5}$$

The indices monitor the type dependence of the parameters, which is important for describing compound systems. The angular dependence is described by

$$g(\theta) = \gamma \left[1 + \frac{c^2}{d^2} - \frac{c^2}{d^2 + (h + \cos\theta)^2} \right]. \tag{6}$$

III. FITTING OF THE FE-PT CROSS POTENTIAL

The general methodology employed in this work for fitting the interatomic potential comprises its adjustment to structural data contained in a fitting database, and has already been described in detail before.[20,23,30] In the case of the Fe-Pt cross potential, the fitting database extends over FePt in the stoichiometric $L1_0$ ordered structure and the ordered structures at compositions Fe_3Pt and $FePt_3$ ($L1_2$). Additionally, special quasirandom structures[31] have been included for fitting the energy difference between the ordered and disordered phases. For complementing the fitting database with structural quantities not available from experiments, total energy calculations in the framework of the density functional theory (DFT) have been carried out, as described in the following.

A. Total energy calculations

The DFT calculations were performed with the Vienna *ab initio* simulation package (VASP).[32] We employed the projector-augmented wave (PAW) method[33,34] and the generalized gradient approximation (GGA) by Perdew and Wang[35] (PW91). For comparison, calculations on $L1_0$ ordered FePt have also been performed within the local density approximation (LDA).[36,37] The plane-wave cutoff energy was set to 348.3 eV. The number of k points in the irreducible Brillouin zone was chosen to guarantee a convergence of the total energy better than 1 meV/atom. A typical value is 360 k points for $L1_0$ ordered FePt.

Minimum energies, lattice constants, as well as bulk moduli and their pressure derivatives have been determined by fitting energy-volume data to the Birch-Murnaghan equation of state.[38] For the $L1_0$ structure, the c/a ratio was identified by calculating energy-volume curves for different fixed c/a ratios and subsequently fitting a second order polynomial to the energy minima. Magnetic ground states were identified by performing non-spin-polarized (nonmagnetic) as well as spin-polarized calculations with ferromagnetic (FM) and antiferromagnetic (AFM) alignment of the atomic spins. Second order elastic constants were calculated by analyzing the deformation energy in response to different deformation modes. The results of the calculations are summarized in Table II. The DFT calculations predict FM ground states for FePt alloys in all the $L1_0$ and $L1_2$ ordered structures. Note, however, that for $L1_2$-$FePt_3$ the energy difference between the FM and AFM states is only 4 meV/atom, and in contrast to the present study, an AFM ground state has been reported in Ref. 39.

For the $L1_0$ ordered compound, our DFT calculations give a formation energy of −224 meV/atom. This is in good agreement with the first principles calculations reported in Ref. 39, where a value of −287 meV/atom is found. In contrast, a thermodynamic assessment of the FePt phase diagram provides a much higher formation energy of −730 meV/atom.[25,40]

The elastic constants of the $L1_0$ FePt phase estimated by LDA and GGA differ from each other, with LDA giving distinctly higher values than GGA. However, the order of the $L1_0$ elastic constants is conserved when switching between

the two approximations, with $c_{11}<c_{33}$, $c_{12}>c_{13}$, and $c_{44}<c_{66}$. Also, in both cases, the elastic constants fulfill the stability criteria for the tetragonal symmetry.[41]

B. Fitting of the order-disorder transition temperature

For fitting the potential to the order-disorder transition temperature T_c at an equiatomic composition, it is desirable to include a disordered random structure in the fitting database. This allows us to control the energy difference between the ordered and the disordered alloys. In order to be representative of the bonding characteristics of infinite, perfectly random alloys, a large number of atoms have to be included in a finite, periodic cell. However, too large structures would significantly reduce the efficiency of the fitting procedure. A good compromise between low computational cost and an exact description of a random alloy is provided by the so-called special quasirandom structures (SQSs).[31] They are specially designed in order to match the first few radial correlation functions of a perfectly random alloy by a small number of atoms. Therefore, a SQS allows us to efficiently capture the most important bonding characteristics in random alloys. The SQS added to the fitting database for the mixed FePt potential consists of 16 atoms (SQS16) and is taken from Ref. 42.

The $L1_0$ and SQS16 structures are only representative of the ordered phase at 0 K and the disordered phase at infinite temperature, respectively. At finite temperatures, a certain degree of disorder in the form of antisite defects is present in the $L1_0$ phase. On the other hand, the $A1$ phase is not perfectly random, but is characterized by a temperature dependent presence of short range order. The degree of order in both phases at the transition temperature is *a priori* unknown. Additionally, a transition from the ferromagnetic to the paramagnetic state occurs at approximately 750 K.[12] Therefore, magnetic energy and entropy contributions to the free energy have to be considered. The latter is, however, missing in the DFT data, and the classical potential description does not properly account for both. On the other hand, there is currently no efficient scheme established that allows us to study both lattice and spin dynamics of nanoparticles at the same time. For these reasons, we resort to a classical description of this magnetic system. Since magnetic entropy contributions are missing in classical molecular dynamics simulations, the static energy differences of the fully ordered and disordered structures as obtained from DFT calculations cannot be used as reference data for the potential fitting. In order to reproduce the correct $L1_0$ to $A1$ transition temperature, the target energy difference ΔE between the SQS16 and the $L1_0$ was therefore taken as an adjustable parameter and has been determined as described in the following.

For parametrizations of the mixed FePt potential fitted to different values of ΔE, the transition temperature was calculated by a series of off-lattice MC simulations in the N, $P=0$, T ensemble. Trial steps consisted of exchanges of two randomly chosen atoms, small random displacements of individual atoms, and random changes of cell dimensions independently in x, y, and z directions. System sizes were chosen from $6\times6\times6$ unit cells (864 atoms) up to $12\times12\times12$ unit cells (6912 atoms). By running simulations at different temperatures and by monitoring a long range order (LRO) parameter as defined in Ref. 16 over an extended interval of MC steps, the transition temperature of a given parametrization has been determined and ΔE was then adjusted accordingly. From these calculations, a ΔE of 0.18 eV has been obtained.

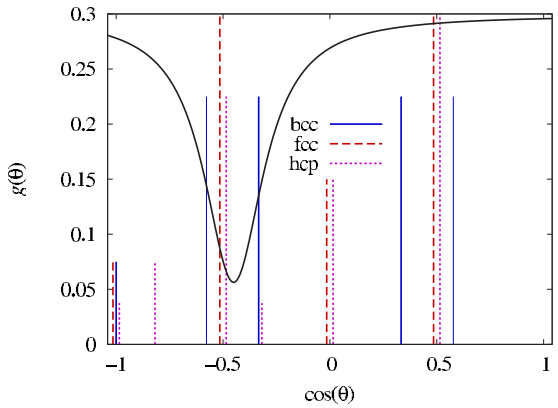

FIG. 1. (Color online) Angular function $g(\theta)$ of the FePt potential. Angles appearing in different structures are indicated by vertical lines. The height of a line is proportional to the weight of the angle in the respective structure. The angles are shifted slightly so that structures having identical angles can be distinguished.

One important side effect of these MC simulations is that they allow the detection of spurious minima in the potential energy landscape that stabilize other configurations over the desired $L1_0$ ground-state structure. If the cutoff distance was restricted to nearest neighbor interactions only, the $B2$ structure was always favored over the desired $L1_0$ ground state. In order to avoid unwanted minimum structures, the cutoff radius of the Fe-Pt cross interactions had to be increased to fully include the second nearest neighbor sphere.

C. Twinning energy

An important value for structure formation in FePt alloys is the twinning energy γ_{twin}, as it determines, for example, the tendency of twinning in nanoparticles. A target value for γ_{twin} in the $L1_0$ phase is available from electronic-structure calculations, which predict an energy of $\gamma_{\text{twin}}=6.5$ meV/Å^2.[43] For the case of Pt, which has a high twinning energy of $\gamma_{\text{twin}}=10$ meV/Å^2,[44] we could show that the magnitude of γ_{twin} can be tuned by carefully positioning the minimum of the function $g(\theta)$ [Eq. (6)] through the parameter h.[21] For the Fe-Pt cross potential, however, we found that h has to be restricted to a narrow range around the value of 0.5. For other values of h, an orthogonal distortion of the $L1_0$ structure with $a\neq b\neq c$ occurred.

The angular dependence of the $g(\theta)$ function of the final Fe-Pt cross potential is shown in Fig. 1. For clarity, bond angles that appear in different structures—such as fcc, hexagonal close packed (hcp), and body centered cubic (bcc)—are also indicated. The position of the minimum of $g(\theta)$ implies an increased bond order in a fcc compared to a hcp environment. Therefore, the hcp structure is disfavored, lead-

TABLE I. Parameter sets for the Fe-Fe, Pt-Pt, and Fe-Pt interaction potentials.

	Interaction type		
Parameter	Pt-Pt (Ref. 21)	Fe-Fe (Ref. 22)	Fe-Pt
D_0 (eV)	1.5	3.2	2.64759104
r_0 (Å)	2.29	2.42	2.36130052
β (Å^{-1})	1.4	1.61	1.45616698
S	2.0693109	2.2955906	2.26243642
γ	0.0115751	0.1854649	0.05633499
c	1.2898716	0.0609071	0.35073555
d	0.3413219	0.08	0.16902364
h	−0.26	0.455	0.45035775
2μ (Å^{-1})	0.0	1.5856477	0.95780361
R (Å)	3.15	3.75	4.20
D (Å)	0.2	0.2	0.20

ing to a high twinning energy in FePt alloys in the present potential, similar to the pure Pt interactions.

The final best-fit parameter set for the Fe-Pt cross potential is given in Table I, together with the parametrizations of the pure Fe and Pt interactions. The properties of the FePt potential are summarized in the following.

IV. CHARACTERIZATION OF THE FE-PT POTENTIAL

A. Structural properties

In Table II, structural properties of FePt in ordered and disordered phases, as obtained from our potential, are compared with literature data and results of our DFT calculations. For comparison, the recent modified embedded atom method (MEAM) potential for FePt by Kim *et al.* is also included.[25] All crystallographic parameters, such as lattice constant and c/a ratio, are in excellent agreement with reference values from literature. For fitting the formation energies of the ordered compounds, the reference values from our total energy calculations have been employed. For obtaining a better agreement of the elastic constants, a deviation of the formation energies toward higher values has been accepted. The final values are, however, still well below the MEAM potential, where formation energies from a thermodynamic assessment of the FePt phase diagram were taken as reference. The formation energies of the $L1_2$ phases are almost identical. We therefore do not expect to reproduce the asymmetry of the full FePt phase diagram, where the Fe_3Pt phase has a much lower ordering temperature than the $FePt_3$ phase. The bulk moduli and elastic constants predicted by the ABOP are in good agreement with the target values. Moreover, the ordering of the elastic constants of the $L1_0$ structure ($c_{11}<c_{33}$, $c_{12}>c_{13}$, and $c_{44}<c_{66}$), as obtained from the total energy calculations, is reproduced by the ABOP.

B. Order-disorder transition

From experimental studies on the FePt phase diagram, a $L1_0$ to $A1$ order-disorder transition temperature of $T_c=1573$ K is reported.[12] For the nature of the transition, strong experimental evidence exists for a first order phase transition: The derivative of the LRO parameter has a discontinuity at T_c,[46] and the transitions between both phases proceed via nucleation and growth.[46–48] Also, two phase regions separating the $L1_0$ and $A1$ phases have been identified.[46–48]

For characterizing the $L1_0$ to $A1$ transition of the FePt ABOP, the LRO parameter has been determined by the MC method as described in the previous section. Close to the transition temperature, the MC data have been sampled with a resolution of 5 K using system sizes up to $12\times12\times12$ unit cells. The resulting evolution of the LRO parameter is shown in Fig. 2. The LRO parameter shows a clear drop, indicating a first order phase transition. The transition temperature as described by the ABOP can be located at 1595(5) K, which is only a slight overestimation of the experimental T_c (1573 K). The possibility of finite size smearing[49] in the present MC data is indicated by the nonvanishing, fluctuating LRO parameter beyond T_c. In systems of a limited number of atoms, small variations of the atomic configuration can lead to relatively high amplitudes in the LRO parameter.

C. Melting temperature

The melting point of an equiatomic FePt alloy predicted by the ABOP has been determined by molecular dynamics simulations of a solid-liquid interface in the N, $P=0$, T ensemble. For increasing temperatures, the position of the solid-liquid interface has been monitored and the melting temperature was found for the zero velocity of the interface, i.e., when the volume fractions of the solid and liquid phases remained constant over the simulation time of 1 ns. As listed in Table III, the melting point estimated by this method is 2050(50) K, which is about 200 K higher than the experimental value of 1873 K.[51] Considering that the potentials for the pure Fe and Pt boundary phases also overestimate the melting temperature, an increased value can be expected and the agreement is still reasonable.

D. Surface and twin-boundary energies

Calculated surface and twin-boundary energies for the $L1_0$ and $A1$ phases are given in Table III. In the $L1_0$ ordered phase, the (111), (100), and (010) surfaces consist of an equal number of Fe and Pt atoms. In contrast, a (001) surface can be occupied either solely by Fe or solely by Pt atoms. In a computational cell with an equiatomic composition and open boundaries along the c direction, both types of (001) surfaces are always contained. Their energies therefor cannot be separated, and an average value is given in Table III. Reference values for surface energies in the $L1_0$ ordered phase are available from DFT calculations.[50] On average, a good performance of the ABOP in describing surface energies is obtained. While the potential reproduces the average (001) surface energy in the $L1_0$ phase, the values for the (111) and (100) surfaces are approximately 18% lower as compared to the results obtained from DFT calculations.

TABLE II. Comparison of structural and cohesive properties of FePt in various phases from calculation and experiment. For the DFT calculations, the parameters are given for the lowest energy magnetic configuration, as indicated. a_0: lattice constant (Å); c/a: axial ratio; E_c: cohesive energy (eV/atom); ΔE_f: energy of formation (eV/atom); B, B': bulk modulus (GPa) and its pressure derivative; c_{ij}: elastic constants (GPa).

	PAW GGA	PAW LDA	Literature	ABOP	MEAM (Ref. 25)
$L1_0$ FePt, ferromagnetic					
a_0	3.872	3.772	3.85[a]	3.862	3.81
c/a	0.973	0.975	0.964[a]	0.963	0.963
ΔE_f	−0.224	−0.140	−0.73[b], −0.29[c]	−0.320	−0.604
E_c	−5.249	−5.165		−5.345	
B	200	251		217	232
B'	5.0	4.2		5.9	
c_{11}	261	360		258	304
c_{33}	299	371		293	242
c_{12}	169	229		203	223
c_{13}	151	185		185	197
c_{44}	103	143		141	107
c_{66}	133	192		182	41
$A1$ random FePt					
a_0			3.80[a]	3.819	3.78
ΔE_f				−0.169	−0.440
E_c				−5.194	
B				214	234
B'				5.5	
c_{11}				257	291[d]
c_{12}				193	205[d]
c_{44}				132	95[d]
$L1_2$ Fe_3Pt, ferromagnetic					
a_0	3.740		3.72[a]	3.73	3.70
ΔE_f	−0.068			−0.234	−0.422
E_c	−4.720			−4.886	
B	174			201	202
B'	3.5			6.0	
c_{11}				259	239
c_{12}				172	184
c_{44}				145	95
$L1_2$ $FePt_3$, ferromagnetic					
a_0	3.924		3.87[a]	3.876	3.84
ΔE_f	−0.188			−0.236	−0.461
E_c	−5.585			−5.634	
B	222			246	256
B'	5.1			5.3	
c_{11}				305	326
c_{12}				217	230
c_{44}				127	90

[a]Reference 12.
[b]Thermodynamic assessment, Ref. 40.
[c]First principles calculations, Ref. 39.
[d]Reference 45.

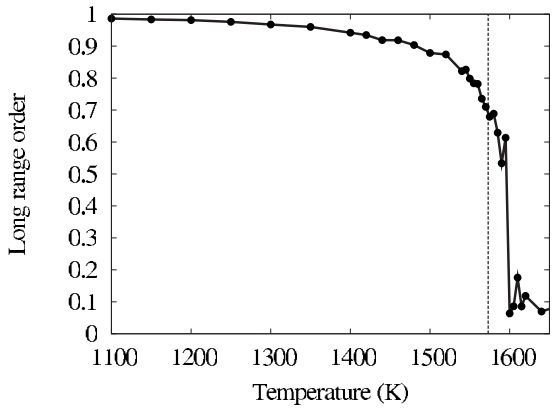

FIG. 2. Variation of the LRO parameter for the $L1_0$ to $A1$ transition with temperature, as obtained by MC simulations for the FePt ABOP. The dashed line indicates the transition temperature of T_c =1573 K reported from experiments (Ref. 12).

Thus, for the random phase, where no reference values are available, a small underestimation of surface energies can also be expected.

For the twin-boundary energies (γ_{twin}) in the $L1_0$ ordered and $A1$ disordered FePt phases, almost identical values of $\gamma_{\text{twin}}=11.7$ meV/Å^2 are obtained. In both phases, the twin boundary is occupied by an equal amount of Fe and Pt atoms, and similar values for γ_{twin} therefore occur naturally. Furthermore, considering the high twin-boundary energy of 10 meV/Å^2 in pure Pt,[44] a high energy penalty for twinning can also be expected in FePt alloys. As discussed in Sec III C, in consequence of the constraint applied to the parameter h, the Fe-Pt cross-interaction potential gives a considerable contribution to γ_{twin} in mixed phases. Therefore, twinning energies with a magnitude similar to pure Pt are obtained. As a reference, electronic-structure calculations give only a value of $\gamma_{\text{twin}}=6.5$ meV/Å^2 for the $L1_0$ ordered phase.[43] These calculations therefore suggest that γ_{twin} in FePt alloys rather scales linearly with the Pt content. In the current potential description, the twinning energy might therefore be overestimated by roughly a factor of 2.

In summary, comparing the properties of the potential with reference data from experiment and *ab initio* calculations demonstrates that the ABOP provides a solid description of FePt alloys. Especially, closely reproducing structural properties, surface energies, and the order-disorder transition temperature in bulk materials, it provides the necessary means for investigating the effects of particle size on the $L1_0$ to $A1$ transition, as described in the following part of this paper.

TABLE III. Comparison of the melting point, surface properties, and twinning energies in FePt predicted by the ABOP with literature data. T_m: melting point (K); $\gamma_{(hkl)}$: energy of (hkl) surface (meV/Å^2); γ_{twin}: (111) twin-boundary energy (meV/Å^2).

	Literature	ABOP
T_m	1873[a]	2050(50)
Ordered $L1_0$ phase		
γ_{100}	132[b]	109
γ_{001} (average)	136[b]	134
γ_{111}	109[b]	89
γ_{twin}	6.5[c]	11.7
Disordered $A1$ phase		
γ_{100}		104
γ_{110}		109
γ_{111}		81
γ_{twin}		11.7

[a]Reference 12.
[b]DFT calculations, Ref. 50.
[c]Electronic-structure calculations, Ref. 43.

V. ORDER-DISORDER TRANSITION IN FePt PARTICLES

The influence of particle size on the order-disorder transition was investigated by means of MC calculations. Particles with diameters of 4 and 5 nm (approx. 2500 and 4000 atoms, respectively) have been considered. These represent the lower size limit for FePt nanoparticles designated for hard magnetic applications: the superparamagnetic limit, where the magnetization becomes thermally unstable, is reached for particles smaller than approximately 4 nm, estimated based on a magnetocrystalline anisotropy energy of the $L1_0$ phase of 7×10^7 erg/cm^3.[1]

The MC simulations used the same algorithm described in Sec. III B, with the exclusion of trial steps that change the size of the simulation cell. To enable a direct comparison with our previous calculations based on an Ising-type lattice Hamiltonian,[16] a regular truncated octahedral shape of the particles has been assumed. Note, however, that from the high ratio of the (100) to (111) surface energies of the FePt $A1$ phase listed in Table III, the Wulff construction (see, e.g., Ref. 52) predicts an equilibrium shape with smaller (100) facets than in the regular truncated octahedron. For assuring that changes in the facet sizes do not alter the results significantly, particles with the correct Wulff shape have also been included in the calculations. Noncrystalline particles with multiply twinned icosahedral or decahedral morphologies can safely be excluded because the large twinning energy renders these structures thermodynamically unfavorable.

A. Lowering of the transition temperature

The order-disorder transition in FePt nanoparticles is investigated by MC calculations monitoring the LRO parameter over a wide temperature range. The temperature variation of the LRO parameter for regular truncated octahedral nanoparticles is depicted in Fig. 3. Within the statistical error, simulations employing the correct Wulff shape lead to the same result and are therefore not discussed separately in the following. For comparison, results of our previous Ising-type Hamiltonian study are also given.[16] Two general trends, both in the Ising model and the ABOP description, are clearly visible: With decreasing particle size, the transition from the ordered to the disordered phase is shifted toward lower temperatures and becomes continuous. At moderate

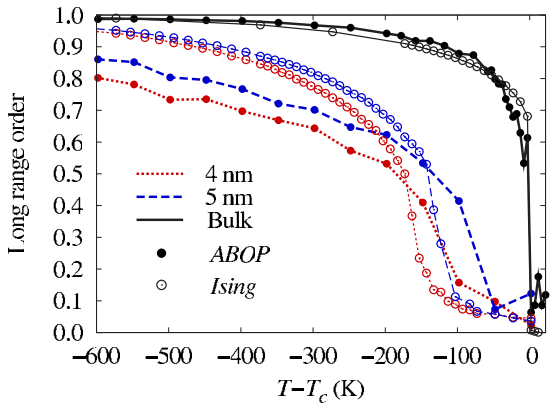

FIG. 3. (Color online) Variation of LRO parameter with temperature in FePt nanoparticles compared to the bulk phase. Data obtained from the ABOP and from an Ising-type lattice Hamiltonian (Ref. 16) are plotted. The temperature axis is taken relative to the order-disorder transition temperature in the bulk phase (T_c). The particle shape is regular truncated octahedral.

temperatures, the amount of ordering in particles is clearly reduced as compared to the bulk FePt phase. However, in no case do the observed effects point to a thermodynamic suppression of ordering at typical annealing temperatures of 800 K below the bulk phase transition temperature.

Interestingly, in the continuum ABOP description, the shift of the order-disorder transition temperature with decreasing particle size is even less pronounced than for the Ising-type lattice Hamiltonian. By taking the highest slope of the curves in Fig. 3 as a measure for the transition temperature, the depression of ordering temperature is roughly 80 K for the 5 nm particle and 120 K for the 4 nm particle. For the Ising-type Hamiltonian, the values are 120 K at 5 nm and 160 K at 4 nm. These small differences between the two models indicate that the lattice strain arising from the tetragonal distortion of the $L1_0$ structure does not significantly affect the depression of the ordering temperature.

Although the ABOP predicts a slightly less pronounced depression of the transition temperature, Fig. 3 shows that the equilibrium degree of order at moderate temperatures predicted by the ABOP is lower than in the Ising-type model. At 1000 K (which is ~600 K below the bulk transition), with only 85% in particles of 5 nm and only 80% in particles of 4 nm, the degree of ordering is clearly reduced in the ABOP. In contrast, with more than 95% ordering for both particle sizes, the Ising-type model predicts significantly higher values for the LRO parameter at the same temperature. As demonstrated in the following, this difference arises from surface contributions to the disorder, which are of different magnitudes in the two models.

B. Surface induced disorder

In Fig. 4, snapshots of 5 nm particles from simulation runs at 1000 K are compared. The cross sections through the particle centers in the bottom row of Fig. 4 demonstrate that, for the ABOP as well as the Ising-type model, a complete order is preserved in the particle volume. In both cases, the

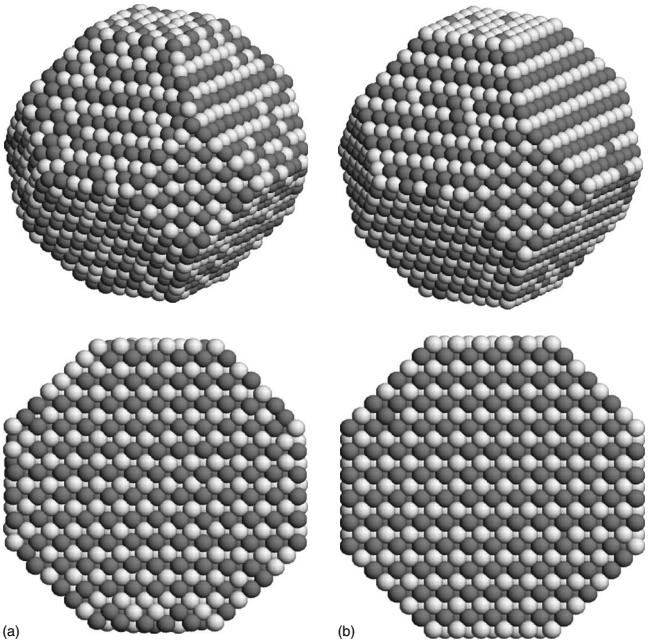

FIG. 4. Snapshots of ~5 nm particles from MC simulations at 1000 K for (a) the ABOP and (b) the Ising-type Hamiltonian. In the bottom row, cross sections through particle centers are shown.

reduced LRO parameter can therefore only be explained by a certain degree of disorder at the particle surface. As can be seen in the top row of Fig. 4, MC simulations employing the ABOP result in a large number of surface antisite defects, leading to an overall reduced LRO parameter. Instead, the Ising-type Hamiltonian only gives rise to a small amount of surface disorder at 1000 K, explaining the higher value of the overall LRO parameter in this case.

Reduced ordering at the particle surface as compared to the volume can be explained by the lower coordination of surface atoms. In the Ising-type Hamiltonian, each broken bond decreases the driving force of an atom to occupy the correct sublattice, while the particle can gain configurational entropy by increasing the disorder. Because of the bond-order dependence, this driving force is even more reduced in the ABOP, which explains the increased surface induced disorder (SID).

In a recent theoretical study on FePt nanoparticles based on a lattice Monte Carlo scheme, Yang *et al.*[17] also identified the presence of SID at temperatures where the particle bulk still remains ordered. They demonstrated that SID is responsible for the pronounced continuous nature of the order-disorder transition in small particles. In the SID mechanism, the disordered layer initiated at the surface grows continually with increasing temperature, eventually transforming the whole particle.

Considering the even higher amount of SID at moderate temperatures, together with the slightly higher transition temperature in the ABOP description, it is interesting to compare how the disorder evolves with temperature in both models. For doing so, LRO parameter profiles of 5 nm particles are plotted for different temperatures in Fig. 5. Following Ref. 17, particles have been divided into layers defined by spherical concentric shells around the particle center. From

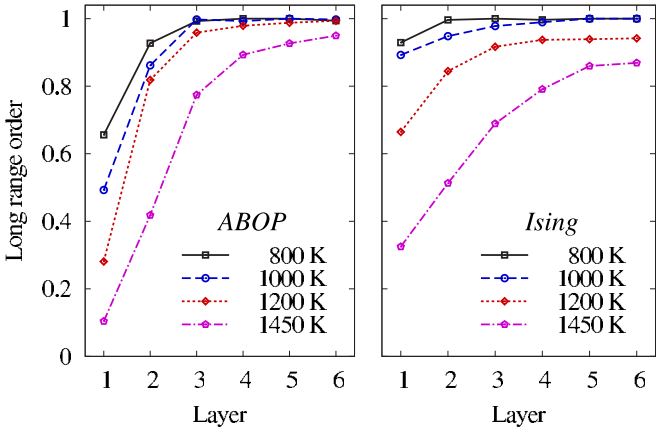

FIG. 5. (Color online) Profiles of LRO parameter for particles of ~5 nm in diameter. Following Ref. 17, a particle is divided into layers based on the distance d from the particle center. Layer 1 contains atoms for which $d \geqslant 2.2$ nm. The subsequent layers 2–5 are shells with width of 0.3 nm each. Finally, layer 6 contains the atoms in the particle core with $d < 1$ nm.

this plot, the differences between the ABOP and the Ising-type model are clearly visible. While the ABOP predicts a higher amount of disorder in surface near regions at all temperatures, the progression of disorder through the particle volume occurs at a lower rate with increasing temperature. At 1450 K, where the average LRO parameter is identical in both models (see Fig. 3), the central layers still remain highly ordered in the ABOP model. In contrast, a clearly reduced ordering is predicted by the Ising-type Hamiltonian within the whole particle, which explains that the transition is completed at somewhat lower temperatures.

VI. SUMMARY

A Fe-Pt cross-interaction potential in the analytic bond-order description is proposed, which includes parametrizations for the boundary phases[22,21] and reproduces structural properties of FePt in the chemically ordered $L1_0$ and $L1_2$ phases, as well as in the $A1$ random alloy phase. The order-disorder transition temperature at an equiatomic composition is well described within the approximately 20 K deviation compared to the experimental transition temperature.

MC simulations based on this potential provide evidence for a slightly reduced order-disorder transition temperature in FePt nanoparticles of 4 and 5 nm diameter. This finding is in line with our previous study based on an Ising-type lattice Hamiltonian.[16] Most notably, however, the ABOP predicts a higher amount of surface induced disorder, reducing the overall LRO parameter by up to 20% at a moderate temperature of 1000 K. On the other hand, including strain effects by the nonideal c/a ratio of the $L1_0$ phase does not prove to have a significant influence on the results. In the investigated 4 nm and 5 nm particles, the ordering transition is even located at slightly higher temperatures, compared to our previous study. The close agreement between the results obtained in the present work as well as in various studies employing coarse grained lattice Hamiltonians[14–17] demonstrates the usefulness of these simple models for investigating size effects in alloy nanoparticles.

In conjunction with the questions concerning the experimental findings on FePt nanoparticles, the present calculations support the previous works by giving further evidence that a depression of the thermodynamic ordering temperature below the typical annealing temperatures of 800 K can be ruled out. However, in equilibrium, the ordered core of FePt nanoparticles can be surrounded by an outer shell possessing a much higher degree of disorder than has been anticipated by previous works. As was pointed out in Ref. 17, this disordered shell can have a significant influence on the magnetic properties, leading to a reduction of the magnetocrystalline anisotropy.

ACKNOWLEDGMENTS

The authors wish to thank B. Kraczek and D. Johnson for communicating their calculations on the twin energy in FePt alloys prior to publication. Generous grants of computer time by the Center for Scientific Computing at the Johann Wolfgang Goethe-University, Frankfurt, Germany is gratefully acknowledged.

*mueller@mm.tu-darmstadt.de

[1] D. Weller, A. Moser, L. Folks, M. E. Best, W. Lee, M. F. Toney, M. Schwickert, J. U. Thiele, and M. F. Doerner, IEEE Trans. Magn. **36**, 10 (2000).
[2] T. Suzuki, N. Honda, and K. Ouchi, IEEE Trans. Magn. **35**, 2748 (1999).
[3] J. S. Chen, B. C. Lim, Y. F. Ding, and G. M. Chow, J. Magn. Magn. Mater. **303**, 309 (2006).
[4] S. Sun, C. B. Murray, D. Weller, L. Folks, and A. Moser, Science **287**, 1989 (2000).
[5] S. Sun, Adv. Mater. (Weinheim, Ger.) **18**, 393 (2006).
[6] B. Bian, Y. Hirotsu, K. Sato, T. Ohkubo, and A. Makino, J. Electron Microsc. **48**, 753 (1999).
[7] Y. K. Takahashi, T. Koyama, M. Ohnuma, T. Ohkubo, and K. Hono, J. Appl. Phys. **95**, 2690 (2004).
[8] S. Stappert, B. Rellinghaus, M. Acet, and E. F. Wassermann, J. Cryst. Growth **252**, 440 (2003).
[9] Z. R. Dai, S. Sun, and Z. L. Wang, Nano Lett. **1**, 443 (2001).
[10] B. Stahl *et al.*, Phys. Rev. B **67**, 014422 (2003).
[11] Y. K. Takahashi, T. Ohkuba, M. Ohnuma, and K. Hono, J. Appl. Phys. **93**, 7166 (2003).
[12] H. Ullmaier, ed., *Binary Systems*, Landolt-Börnstein, New Series, Group 4, Physical Chemistry, Vol. IV (Springer-Verlag, Heidelberg, 1991).
[13] O. Dmitrieva, B. Rellinghaus, J. Kästner, M. O. Liedke, and J. Fassbender, J. Appl. Phys. **97**, 10N112 (2005).
[14] B. Yang, M. Asta, O. N. Mryasov, T. J. Klemmer, and R. W. Chantrell, Scr. Mater. **53**, 417 (2005).

[15] R. V. Chepulskii and W. H. Butler, Phys. Rev. B **72**, 134205 (2005).
[16] M. Müller and K. Albe, Phys. Rev. B **72**, 094203 (2005).
[17] B. Yang, M. Asta, O. N. Mryasov, T. J. Klemmer, and R. W. Chantrell, Acta Mater. **54**, 4201 (2006).
[18] A. Kovács, K. Sato, G. Sáfrán, P. B. Barna, and Y. Hirotsu, Philos. Mag. **84**, 2075 (2004).
[19] C. Y. Tan, J. S. Chen, B. H. Liu, and G. M. Chow, J. Cryst. Growth **293**, 175 (2006).
[20] K. Albe, K. Nordlund, and R. S. Averback, Phys. Rev. B **65**, 195124 (2002).
[21] M. Müller, P. Erhart, and K. Albe .J. Phys.: Condens. Matter **19**, 326220 (2007)
[22] M. Müller, P. Erhart, and K. Albe (unpublished).
[23] N. Juslin, P. Erhart, P. Traskelin, J. Nord, K. Henriksson, K. Nordlund, E. Salonen, and K. Albe, J. Appl. Phys. **98**, 123520 (2005).
[24] P. Erhart, N. Juslin, O. Goy, K. Nordlund, R. Müller, and K. Albe, J. Phys.: Condens. Matter **18**, 6585 (2006).
[25] J. Kim, Y. Koo, and B. J. Lee, J. Mater. Res. **21**, 199 (2006).
[26] G. C. Abell, Phys. Rev. B **31**, 6184 (1985).
[27] J. Tersoff, Phys. Rev. B **37**, 6991 (1988).
[28] D. W. Brenner, Phys. Rev. Lett. **63**, 1022 (1989).
[29] D. W. Brenner, Phys. Rev. B **42**, 9458 (1990).
[30] K. Albe, K. Nordlund, J. Nord, and A. Kuronen, Phys. Rev. B **66**, 035205 (2002).
[31] S. H. Wei, L. G. Ferreira, J. E. Bernard, and A. Zunger, Phys. Rev. B **42**, 9622 (1990).
[32] G. Kresse and J. Furthmüller, Phys. Rev. B **54**, 11169 (1996).
[33] P. E. Blöchl, Phys. Rev. B **50**, 17953 (1994).
[34] G. Kresse and D. Joubert, Phys. Rev. B **59**, 1758 (1999).
[35] J. P. Perdew, in *Electronic Structure of Solids*, edited by P. Ziesche and H. Eschrig (Akademie, Berlin, 1991).
[36] D. M. Ceperley and B. J. Alder, Phys. Rev. Lett. **45**, 566 (1980).
[37] J. P. Perdew and A. Zunger, Phys. Rev. B **23**, 5048 (1981).
[38] F. Birch, J. Geophys. Res. **83**, 1257 (1978).
[39] Y. Chen, S. Iwata, and T. Mohri, CALPHAD: Comput. Coupling Phase Diagrams Thermochem. **26**, 583 (2002).
[40] P. Fredriksson and B. Sundman, CALPHAD: Comput. Coupling Phase Diagrams Thermochem. **25**, 535 (2001).
[41] O. Beckstein, J. E. Klepeis, G. L. W. Hart, and O. Pankratov, Phys. Rev. B **63**, 134112 (2001).
[42] A. V. Ruban, S. I. Simak, S. Shallcross, and H. L. Skriver, Phys. Rev. B **67**, 214302 (2003).
[43] B. Kraczek and D. D. Johnson (private communication); G. Brown, B. Kraczek, A. Janotti, T. C. Schulthess, G. M. Stocks, and D. D. Johnson, Phys. Rev. B **68**, 052405 (2003).
[44] N. Bernstein and E. B. Tadmor, Phys. Rev. B **69**, 094116 (2004).
[45] J. S. Kim, Y. M. Koo, B. J. Lee, and S. R. Lee, J. Appl. Phys. **99**, 053906 (2006).
[46] S. H. Whang, Q. Feng, and Y. Q. Gao, Acta Mater. **46**, 6485 (1998).
[47] A. Kußmann and G. von Rittberg, Z. Metallkd. **41**, 470 (1950).
[48] M. Toney, W. Lee, J. Hedstrom, and A. Kellock, J. Appl. Phys. **93**, 9902 (2003).
[49] O. G. Mouritsen, *Computer Studies of Phase Transitions and Critical Phenomena* (Springer-Verlag, Berlin, 1984).
[50] S. Hong and M. H. Yoo, J. Appl. Phys. **97**, 084315 (2005).
[51] P. Ehrhart, *Binary Systems*, Landolt-Börnstein, New Series, Group 4, Physical Chemistry, Vol. III (Springer-Verlag, Heidelberg, 1991).
[52] F. Baletto and R. Ferrando, Rev. Mod. Phys. **77**, 371 (2005).